

Particle generation through restrictive planes in GEANT4 simulations for potential applications of cosmic ray muon tomography

A. Ilker Topuz^{1,2}, Madis Kiisk^{1,3}, Andrea Giammanco²

¹Institute of Physics, University of Tartu, W. Ostwaldi 1, 50411, Tartu, Estonia

²Centre for Cosmology, Particle Physics and Phenomenology, Université catholique de Louvain, Chemin du Cyclotron 2, B-1348 Louvain-la-Neuve, Belgium

³GScan OU, Maealuse 2/1, 12618 Tallinn, Estonia

Abstract

In this study, by attempting to resolve the angular complication during the particle generation for the muon tomography applications in the GEANT4 simulations, we exhibit an unconventional methodology that is hinged on the direction limitation via the vectorial construction from the generation location to the restriction area rather than using a certain angular distribution or interval. In other words, we favor a momentum direction that is determined by a vector constructed between an initial point randomly chosen on a generative point/plane and a latter point arbitrarily selected on a restrictive plane of the same dimensions with the basal cross section of the volume-of-interest (VOI). On account of setting out such a generation scheme, we optimize the particle loss by keeping an angular disparity that is directly dependent on the VOI geometry as well as the vertical position of the restrictive plane for a tomographic system of a finite size. We demonstrate our strategy for a set of target materials including aluminum, copper, iron, lead, and uranium with a dimension of $40 \times 10 \times 40 \text{ cm}^3$ over three restrictive planes of different positions by using a discrete energy spectrum between 0.1 and 8 GeV and we compute the scattering angle, the number of absorption, and the particle loss. Upon our simulation outcomes, we show that the particle generation by means of restrictive planes is an effective strategy that is flexible towards a variety of computational objectives in the GEANT4 simulations.

Keywords: Muon tomography; Characteristic parameters; Restrictive planes; Source biasing; Non-analogue Monte Carlo simulations; GEANT4

1 Introduction

The wide angular distribution [1] of the incoming cosmic ray muons in connection with either incident angle or azimuthal angle is a challenging trait that leads to a drastic particle loss in the course of parametric computations through the GEANT4 [2] simulations associated with the muon tomography [3–5] since the tomographic configurations as well as the target geometries also influence the processable number of the detected particles apart from the generation strategies. To further detail, the basic parameters such as the scattering angle, the particle displacement, and the particle absorption owing to the volume-of-interest (VOI) *de facto* dictate the particle penetration through the multiple sections of the tomographic setup in addition to the VOI. Hence, a number of the loss cases notably come into effect unless the calculation conditions are fulfilled, and not only the computation statistics as well as the numerical outcomes but the initial assumptions like the energy spectrum are also perturbed since the VOI accepts a significantly lower number of particles in the instance of the substantial particle loss. While a number of source biasing techniques [6] are offered by MCNP6 [7, 8] in the black box format under the class of non-analogue Monte Carlo simulations, the GEANT4 simulations are usually constrained to the existing particle generators or the general particle source (GPS) unless G4ParticleGun is favored. Motivated by the excessive particle loss and its effect on the computation time as well as the characteristic parameters identified in the muon tomography, we set forth in the present study a scheme that is hinged on the particle generation through the planar restriction by means of the vectorial construction over our tomographic setup consisting of plastic scintillators manufactured from polyvinyl toluene with the dimensions of $100 \times 0.4 \times 100 \text{ cm}^3$. This study is organized as follows. In section 2, we elucidate our methodology based on the restrictive planes and we express our characteristic parameters as well as our simulation features in section 3. While we disclose our simulation outcomes in section 4, we draw our conclusions in section 5.

2 Generation via planar restriction

To begin with, we principally exhibit two planar restrictive schemes to be adapted in GEANT4 as illustrated in Fig. 1 where (a) shows the particle generation from a fixed point as well as the direction restriction by means of a restrictive pseudo-plane, whereas (b) demonstrates the randomly picked up particles from a generative plane, the directions of which are projected into a similar restrictive plane.

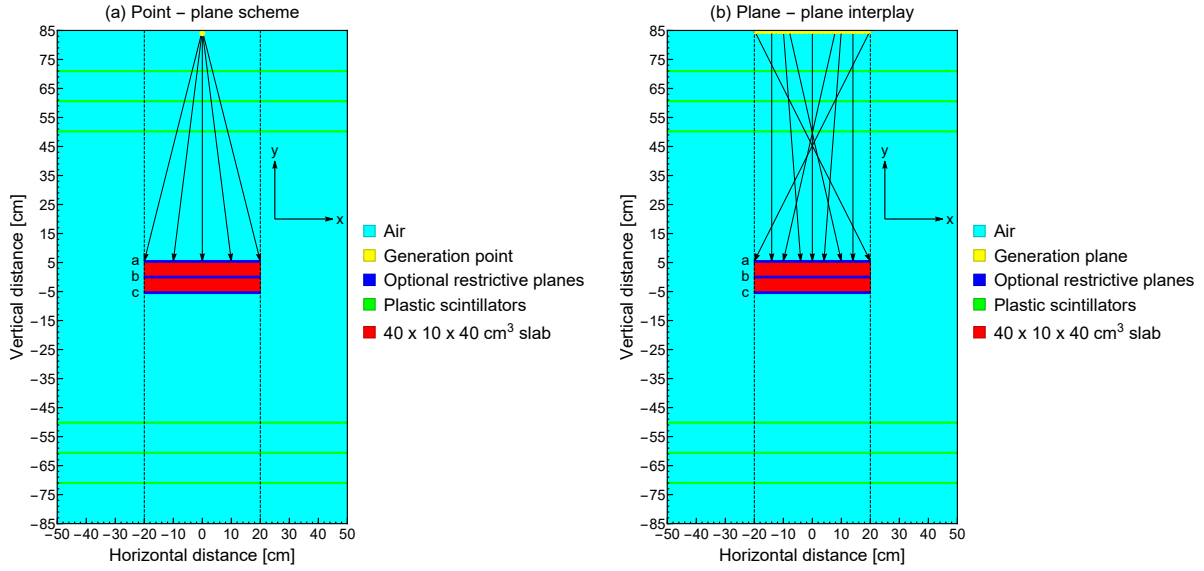


Figure 1: Depiction of particle generation through restrictive planes in GEANT4 (a) generative point - restrictive plane scheme and (b) generative - restrictive planar interplay.

In order to practically outline the present methodology that is initially described in Fig. 1(a), the particle location in cm on the central point at height=85 cm is listed as written in

$$x_0 = 0, \quad y_0 = 85, \quad z_0 = 0 \quad (1)$$

Subsequently, the confined location in cm on any restrictive plane of $2L \times 2D$ cm² is noted as shown in

$$x_1 = -L + 2 \times L \times \text{G4UniformRand}(), \quad y_1 = \text{constant}, \quad z_1 = -D + 2 \times D \times \text{G4UniformRand}() \quad (2)$$

Here, $\text{G4UniformRand}()$ is the uniform random number generator between 0 and 1, which is pre-defined in GEANT4. Then, by constructing a vector from the generative point to the restrictive plane, we obtain

$$px = x_1 - x_0 = x_1, \quad py = y_1 - y_0, \quad pz = z_1 - z_0 = z_1 \quad (3)$$

Thus, the selective momentum direction, i.e. $\vec{P} = (P_x, P_y, P_z)$, is

$$P_x = \frac{px}{\sqrt{px^2 + py^2 + pz^2}}, \quad P_y = \frac{py}{\sqrt{px^2 + py^2 + pz^2}}, \quad P_z = \frac{pz}{\sqrt{px^2 + py^2 + pz^2}} \quad (4)$$

The latter scheme that assumes a planar generation as delineated in Fig. 1(b) entails particle locations in cm on the generative plane of $2L \times 2D$ cm² as written in

$$x_0 = -L + 2 \times L \times \text{G4UniformRand}(), \quad y_0 = 85, \quad z_0 = -D + 2 \times D \times \text{G4UniformRand}() \quad (5)$$

As performed in Eq. 2 for the previous scheme, the limited locations in cm on any restrictive plane of $2L \times 2D$ cm² are selected from

$$x_1 = -L + 2 \times L \times \text{G4UniformRand}(), \quad y_1 = \text{constant}, \quad z_1 = -D + 2 \times D \times \text{G4UniformRand}() \quad (6)$$

Additionally, via a vector construction between two planes, we acquire anew

$$px = x_1 - x_0, \quad py = y_1 - y_0, \quad pz = z_1 - z_0 \quad (7)$$

Therefore, the selective momentum direction denoted by $\vec{P} = (P_x, P_y, P_z)$ is again

$$P_x = \frac{px}{\sqrt{px^2 + py^2 + pz^2}}, \quad P_y = \frac{py}{\sqrt{px^2 + py^2 + pz^2}}, \quad P_z = \frac{pz}{\sqrt{px^2 + py^2 + pz^2}} \quad (8)$$

The initial particle positions and the selective momentum directions are incorporated by using G4ParticleGun . The simulation previews through both the restrictive schemes are displayed in Fig. 2 where (a) indicates the particles generated from a fixed point, while (b) presents the randomly generated particles from a fixed plane.

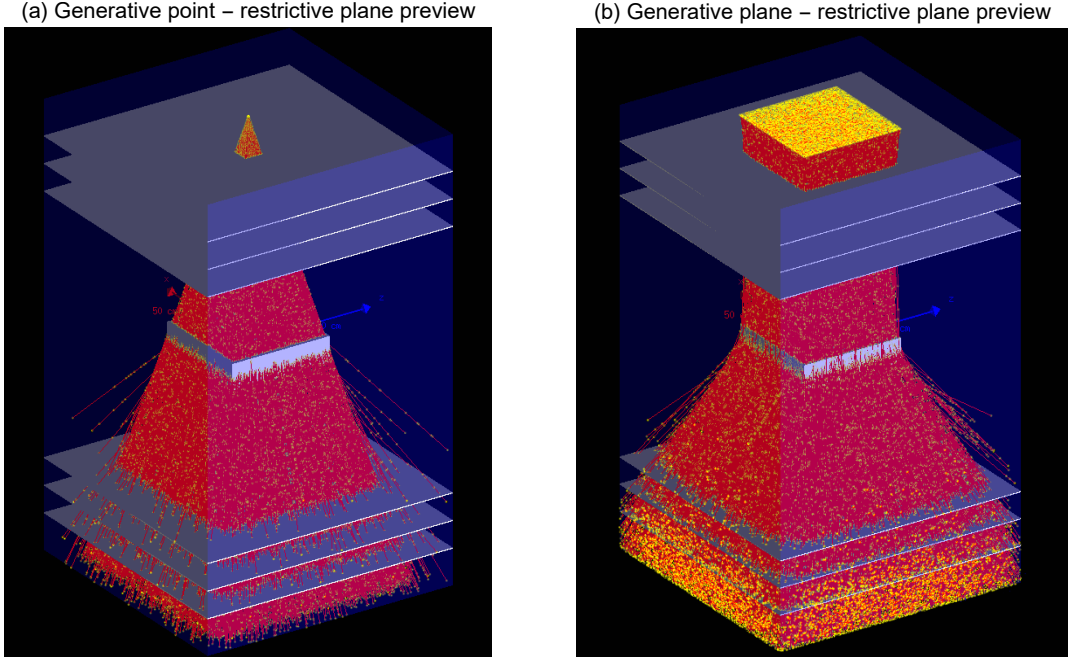


Figure 2: Simulation previews by using restrictive plane b for copper in GEANT4 (a) point - plane scheme and (b) plane - plane scheme.

It is worth mentioning that neither generation points/planes nor restrictive planes are subject to any limitation in terms of shape, size, or location since our recent concept is preferred in the first instance for the sake of simplicity. On top of this, it is also possible to favor different distributions especially already implemented in GEANT4, e.g. Gauss or Poisson distribution depending on the envisaged application.

3 Characteristic parameters and simulation setup

Before getting down to test our schemes, we express our characteristic parameters to be computed in the wake of the GEANT4 simulations. The average scattering angle due to the target volume and its standard deviation over N number of the non-absorbed/non-decayed muons is determined as expressed in [9–11]

$$\bar{\theta} \pm \delta\theta = \frac{1}{N} \sum_{i=1}^N \theta_i \pm \sqrt{\frac{1}{N} \sum_{j=1}^N (\theta_j - \bar{\theta})^2} \quad (9)$$

Additionally, the root-mean-square (RMS) of the scattering angle over N number of the non-absorbed/non-decayed muons is calculated by using the following expression:

$$\theta_{\text{RMS}} = \sqrt{\frac{1}{N} \sum_{i=1}^N \theta_i^2} \quad (10)$$

Along with the scattering angle, we squarely track the number of the absorbed muons within the VOI as denoted in

$$\#_{\text{Capture}}^{\text{In-target}} = \# \text{ of muMinusCaptureAtRest in VOI} \quad (11)$$

Last but not least, we define the particle loss entitled off-target loss as follows

$$\#_{\text{Loss}}^{\text{Off-target}} \approx \underbrace{\#_{\text{Out-scattering}}}_{\text{Characteristic}} + \underbrace{\#_{\text{Decay}}}_{\text{Negligible}} + \underbrace{\#_{\text{Capture}}^{\text{Off-target}}}_{\text{Negligible}} + \underbrace{\#_{\text{Deflection}}^{\text{Initial}}}_{\text{Occasional}} \quad (12)$$

where $\#_{\text{Out-scattering}}$ is the number of the scattered muons from the VOI by leaking out of the tomographic device, $\#_{\text{Decay}}$ is the negligible number of the decayed muons into electrons/positrons, $\#_{\text{Capture}}^{\text{Off-target}}$ is the insignificant number of the absorbed muons outside the VOI, and $\#_{\text{Deflection}}^{\text{Initial}}$ is the number of muons that miss the

VOI only in the case of the wide beams, which occasionally occurs due to the barriers before the VOI despite the initial restricted orientation to the VOI boundary, i.e. the tiny deflection owing to the detector layers.

Table 1: Simulation features.

Particle	μ^-
Momentum direction	Restrictive downward
Beam geometry	Prismatic
Initial position (cm)	y=85
Particle injector	G4ParticleGun
Number of particles	10^5
Energy distribution	Non-linear discrete
Energy interval	[0, 8]
Energy bin step length (GeV)	0.1
Target geometry	Rectangular prism
Target volume (cm ³)	$40 \times 10 \times 40$
Material database	G4/NIST
Reference physics list	FTFP_BERT

Our simulation features are summarized in Table 1, and we use a 80-bin discrete muon energy spectrum extracted from the CRY generator [12] between 0 and 8 GeV. The muon tracking is accomplished by G4Step, and the recorded hit positions on the detector layers are post-processed at the hand of a Python script.

4 Simulation outcomes

We asses our methodology over our tomographic configuration described in Fig. 1(a)-(b) and we select our set of materials and the VOI geometry in accordance with another study [13] dedicated to the muon tomography where the material list consists of aluminum, copper, iron, lead, and uranium, and the target geometry is composed of a rectangular prism with the dimensions of $40 \times 10 \times 40$ cm³. As indicated in Fig. 1, we contrast three restrictive planes labeled as a, b, and c that are placed atop the VOI, amidst the VOI, and beneath the VOI, respectively. We commence with the first scheme that is based on the point - plane generation, and the simulation outcomes by using restrictive plane a are listed in Table 2.

Table 2: Point - plane scheme, restrictive plane a, thickness=10 cm.

Material	$\bar{\theta} \pm \delta\theta$ [mrad]	θ_{RMS} [mrad]	$\#_{\text{Capture}}^{\text{In-target}}$	$\#_{\text{Loss}}^{\text{Off-target}}$
Aluminum	14.890 ± 25.741	29.738	-	516
Copper	37.376 ± 55.515	66.924	1083	616
Iron	32.980 ± 47.420	57.761	1073	541
Lead	59.486 ± 81.898	101.222	1135	1215
Uranium	73.649 ± 91.114	117.158	3267	1542

As shown in Table 2, the computed parameters including the particle loss show a characteristic tendency depending on the atomic number as well as the material density for a fixed thickness. Although the muon beam is already directed to the VOI boundary even in the case of restrictive plane a, which leads to an immoderate reduction in the particle loss compared to the conventional approaches, a remarkable number of the loss events in agreement with the intrinsic properties of the target material are still observed.

Table 3: Point - plane scheme, restrictive plane b, thickness=10 cm.

Material	$\bar{\theta} \pm \delta\theta$ [mrad]	θ_{RMS} [mrad]	$\#_{\text{Capture}}^{\text{In-target}}$	$\#_{\text{Loss}}^{\text{Off-target}}$
Aluminum	15.771 ± 26.427	30.775	-	54
Copper	39.545 ± 56.941	69.326	1179	216
Iron	35.306 ± 50.117	61.304	1172	133
Lead	63.172 ± 84.172	105.241	1220	833
Uranium	78.160 ± 93.551	121.904	3604	1187

In order to see the positional effect of the planar restriction, the simulation outcomes from restrictive plane b are tabulated in Table 3. In comparison with Table 2, we observe that the characteristic parameters except the particle loss slightly change when the muon beam is narrowed by using restrictive plane b; however, the particle loss manifests a minimum reduction of 31% as opposed to restrictive plane a. Whereas restrictive plane b is capable of diminishing the particle loss by a factor of order in certain cases, we still notice that the particle loss remains distinctive among the simulated materials.

By using restrictive plane c, we further decrease the incident angle and we obtain the simulation results as written down in Table 4. In comparison with Table 3, restrictive plane c yields a minuscule change in terms of the characteristic parameters containing the particle loss, which also means that the variation rate of the characteristic parameters is expected to be insignificant beyond restrictive plane c.

Table 4: Point - plane scheme, restrictive plane c, thickness=10 cm.

Material	$\bar{\theta} \pm \delta\theta$ [mrad]	θ_{RMS} [mrad]	$\#_{\text{Capture}}^{\text{In-target}}$	$\#_{\text{Loss}}^{\text{Off-target}}$
Aluminum	16.142 \pm 27.368	31.774	-	35
Copper	40.355 \pm 58.022	70.676	1216	193
Iron	35.916 \pm 50.635	62.080	1215	107
Lead	64.542 \pm 85.965	107.497	1287	793
Uranium	79.700 \pm 96.102	124.850	3764	1059

It is noteworthy to mention that a partial transition from the particle loss to the particle absorption is perceptible according to Tables 2-4 especially if the VOI material is a potent absorber since the low-energy muons that lead to the particle loss in the wide beams typically have the absorption potential when interacting with the VOI material in the narrow beams, which also means that a certain portion of the particle loss is converted into the particle absorption in the VOI material towards restrictive plane c.

Table 5: Plane - plane scheme, restrictive plane a, thickness=10 cm.

Material	$\bar{\theta} \pm \delta\theta$ [mrad]	θ_{RMS} [mrad]	$\#_{\text{Capture}}^{\text{In-target}}$	$\#_{\text{Loss}}^{\text{Off-target}}$
Aluminum	15.196 \pm 26.036	30.146	-	1196
Copper	37.454 \pm 55.612	67.049	1118	1728
Iron	33.375 \pm 48.047	58.502	1092	1575
Lead	59.927 \pm 83.320	102.633	1206	2624
Uranium	74.073 \pm 92.787	118.728	3352	3299

In the next step, we continue with the plane - plane scheme, and Table 5 lists the simulation outcomes for restrictive plane a. In spite of the schematic change, we see that the characteristic parameters excluding the particle loss do not exhibit a significant difference. On the other hand, the particle loss via restrictive plane a within the plane - plane interplay results in the elevated values as displayed in Table 5 in contrast to Tables 2-4.

Table 6: Plane - plane scheme, restrictive plane b, thickness=10 cm.

Material	$\bar{\theta} \pm \delta\theta$ [mrad]	θ_{RMS} [mrad]	$\#_{\text{Capture}}^{\text{In-target}}$	$\#_{\text{Loss}}^{\text{Off-target}}$
Aluminum	16.103 \pm 27.566	31.925	-	138
Copper	39.897 \pm 57.927	70.337	1220	581
Iron	35.380 \pm 50.142	61.367	1206	430
Lead	63.335 \pm 84.573	105.659	1327	1423
Uranium	78.399 \pm 94.631	122.888	3699	1926

So as to demonstrate the impact of the spatial change in the planar restriction for this scheme, the simulation results via restrictive plane b are tabulated in Table 6, and we experience a similar trend compared to the point-plane scheme that induces a drastic diminution in the particle loss along with the tiny variations in the rest of the characteristic parameters. As a means to complete our quantitative investigation for the plane - plane scheme, the simulation results for restrictive plane c are listed in Table 7, and we face a close trend as opposed to Table 4, which also means that the reduction rate in the particle loss is moderated together with the very minor variations in the remaining characteristic parameters.

Table 7: Plane - plane scheme, restrictive plane c, thickness=10 cm.

Material	$\bar{\theta} \pm \delta\theta$ [mrad]	θ_{RMS} [mrad]	$\#_{\text{Capture}}^{\text{In-target}}$	$\#_{\text{Loss}}^{\text{Off-target}}$
Aluminum	16.279 \pm 27.365	31.841	-	88
Copper	40.386 \pm 57.627	70.370	1258	389
Iron	36.135 \pm 50.751	62.300	1249	263
Lead	64.517 \pm 86.095	107.586	1358	1164
Uranium	80.087 \pm 96.225	125.193	3833	1537

In the long run, our last simulations are devoted to investigate the thickness effect by solely using restrictive plane b since we aim at optimizing the particle loss with an ideal angular acceptance. Thus, Table 8 shows the characteristic parameters that are acquired by means of the point - plane scheme as well as restrictive plane b for a thickness of 40 cm with the same material group.

Table 8: Point - plane scheme, restrictive plane b, thickness=40 cm.

Material	$\bar{\theta} \pm \delta\theta$ [mrad]	θ_{RMS} [mrad]	$\#_{\text{Capture}}^{\text{In-target}}$	$\#_{\text{Loss}}^{\text{Off-target}}$
Aluminum	27.849 \pm 37.186	46.458	3046	93
Copper	65.133 \pm 75.969	100.068	11072	588
Iron	58.208 \pm 67.893	89.429	10365	528
Lead	102.566 \pm 112.951	152.570	11036	2210
Uranium	121.060 \pm 121.502	171.517	20371	3084

From Table 8, we numerically demonstrate that all the characteristic parameters increase as a function of thickness, and we find the most notable rise in the particle absorption. Finally, Table 9 lists the simulation results through the plane-plane scheme for the same thickness, and we see that the latter scheme is not significantly different from the initial scheme with regard to the characteristic parameters omitting a higher number of the particle loss.

Table 9: Plane - plane scheme, restrictive plane b, thickness=40 cm.

Material	$\bar{\theta} \pm \delta\theta$ [mrad]	θ_{RMS} [mrad]	$\#_{\text{Capture}}^{\text{In-target}}$	$\#_{\text{Loss}}^{\text{Off-target}}$
Aluminum	28.022 \pm 37.620	46.910	3080	272
Copper	65.229 \pm 77.147	101.026	11341	1184
Iron	58.373 \pm 68.363	89.894	10599	1086
Lead	101.906 \pm 113.230	152.335	11341	3341
Uranium	120.089 \pm 121.872	171.097	20867	4181

5 Conclusion

All in all, by setting out our restrictive generation scheme, we optimize the particle loss by keeping an angular disparity that is directly dependent on the VOI geometry as well as the vertical position of the restrictive plane for a tomographic system of a finite size. Upon our simulation outcomes, we show that the particle generation by means of restrictive planes is an effective strategy that is flexible towards a variety of computational objectives in GEANT4. Into the bargain, we explicitly observe that the off-target loss is a characteristic parameter that varies in an ascending order from aluminum to uranium.

References

- [1] B. O. Yáñez, A. A. Aguilar-Arevalo, A method to measure the integral vertical intensity and angular distribution of atmospheric muons with a stationary plastic scintillator bar detector, Nucl. Instr. Meth. A 987 (2021) 164870.
- [2] S. Agostinelli, J. Allison, K. Amako, J. Apostolakis, H. Araujo, P. Arce, M. Asai, D. Axen, S. Banerjee, G. Barrand, et al., GEANT4—a simulation toolkit, Nuclear instruments and methods in physics research section A: Accelerators, Spectrometers, Detectors and Associated Equipment 506 (3) (2003) 250–303.
- [3] S. Pesente, S. Vanini, M. Benettoni, G. Bonomi, P. Calvini, P. Checchia, E. Conti, F. Gonella, G. Nebbia, S. Squarcia, et al., First results on material identification and imaging with a large-volume muon

tomography prototype, Nuclear Instruments and Methods in Physics Research Section A: Accelerators, Spectrometers, Detectors and Associated Equipment 604 (3) (2009) 738–746.

- [4] S. Procureur, Muon imaging: Principles, technologies and applications, Nucl. Instr. Meth. A 878 (2018) 169.
- [5] L. Bonechi, R. D’Alessandro, A. Giammanco, Atmospheric muons as an imaging tool, Reviews in Physics 5 (2020) 100038.
- [6] J. K. Shultis, R. E. Faw, An MCNP primer, Tech. rep., Manhattan, Kansas State University (2011).
- [7] R. Forster, T. Godfrey, MCNP - a general Monte Carlo code for neutron and photon transport, in: Monte Carlo Methods and Applications in Neutronics, Photonics and Statistical Physics, Springer, 1985, pp. 33–55.
- [8] T. Goorley, M. James, T. Booth, F. Brown, J. Bull, L. Cox, J. Durkee, J. Elson, M. Fensin, R. Forster, et al., Initial MCNP6 release overview, Nuclear technology 180 (3) (2012) 298–315.
- [9] T. Carlisle, J. Cobb, D. Neuffer, Multiple Scattering Measurements in the MICE Experiment, Tech. Rep. FERMILAB-CONF-12-171-APC, Fermi National Accelerator Lab. (FNAL), Batavia, IL (United States) (2012).
- [10] J. C. Nugent, Multiple Coulomb scattering in the MICE experiment, Ph.D. thesis, University of Glasgow (2017).
- [11] D. Poulson, J. Bacon, M. Durham, E. Guardincerri, C. Morris, H. R. Trellue, Application of muon tomography to fuel cask monitoring, Philosophical Transactions of the Royal Society A 377 (2137) (2019) 20180052.
- [12] C. Hagmann, D. Lange, D. Wright, Cosmic-ray shower generator (CRY) for Monte Carlo transport codes, in: 2007 IEEE Nuclear Science Symposium Conference Record, Vol. 2, IEEE, pp. 1143–1146.
- [13] M. Hohlmann, P. Ford, K. Gnanvo, J. Helsby, D. Pena, R. Hoch, D. Mitra, GEANT4 Simulation of a Cosmic Ray Muon Tomography System With Micro-Pattern Gas Detectors for the Detection of High-Z Materials, IEEE Transactions on Nuclear Science 56 (3) (2009) 1356–1363.